

Partial order from disorder in a classical pyrochlore antiferromagnet

Gia-Wei Chern,¹ R. Moessner,² and O. Tchernyshyov¹

¹*Department of Physics and Astronomy, Johns Hopkins University, Baltimore, Maryland 21218, USA*

²*Max-Planck-Institut für Physik komplexer Systeme, 01187 Dresden, Germany*

(Dated: April 10, 2019)

We investigate theoretically the phase diagram of a classical Heisenberg antiferromagnet on the pyrochlore lattice perturbed by a weak second-neighbor interaction J_2 . The huge ground state degeneracy of the nearest-neighbor Heisenberg spins is lifted by J_2 and a ground state with magnetic order sets in as the temperature approaches zero. We have found a new, partially ordered phase with collinear spins that is stable at intermediate temperatures for a ferromagnetic J_2 . In addition to a large nematic order parameter, this intermediate phase also exhibits a layered structure and a bond order that breaks the sublattice symmetry. We analytically examine the stability of the collinear state and obtain a phase boundary $T \sim J_2^2/J_1$ in agreement with Monte Carlo simulations.

I. INTRODUCTION

Magnets with geometrical frustration¹ have received much attention as models of strongly interacting electronic systems with unusual ground states, thermodynamic phases, and excitations. The hallmark of strong frustration is a conspicuously large degeneracy of the classical ground state: essentially, a finite *fraction* of the degrees of freedom remains unconstrained to the lowest temperatures. For discrete spins, this manifests itself in the number of ground states scaling exponentially with the system volume and thus giving rise to a nonzero entropy density at absolute zero temperature. Well-known examples of that are the Ising antiferromagnet on the triangular lattice^{2,3} and spin ice.⁴ For continuous spins — most saliently for the Heisenberg antiferromagnet on the pyrochlore lattice — the classical ground states form a *manifold* with the number of dimensions proportional to the system volume.⁵ In that particular case, the classical model exhibits strong short-range spin correlations but fails to exhibit any form of conventional magnetic order down to the lowest temperatures accessible in Monte Carlo simulations. The strong correlation between the local motions of spins in this liquid-like phase manifests itself as an emergent gauge structure at low energy scales, resulting in a dipolar form of the asymptotic spin correlations.^{6,7}

At the same time, the large degeneracy of the ground state makes this system susceptible to all kinds of perturbations, which certainly exist in real compounds. For instance, the spin-lattice coupling, arising from the dependence of exchange strength on the atomic displacements,⁸ lifts the degeneracy through a spin analog of the Jahn-Teller effect⁹ observed in spinels ZnCr_2O_4 ¹⁰ and CdCr_2O_4 .¹¹

This naturally leads one to ponder the following questions. Can the interplay of a weak perturbation with strong frustration lead to interesting ordered phases? Are there any (intermediate) partially ordered phases? What is the nature of the phase transitions between such phases? In this paper we discuss these questions in the context of a classical Heisenberg antiferromagnet on the

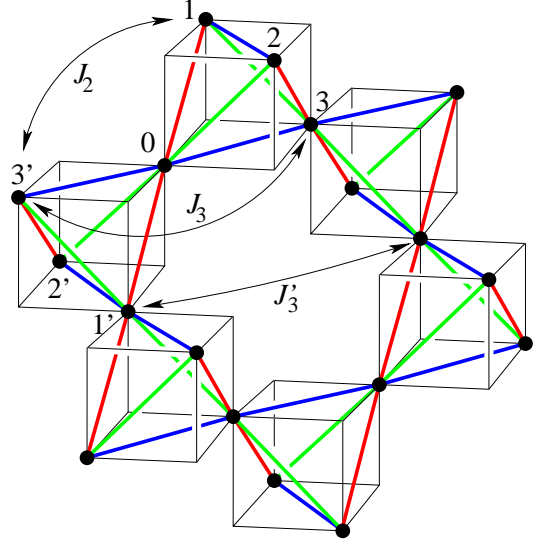


FIG. 1: Second and third-neighbor pairs on the pyrochlore lattice. Since exchange paths giving rise to J_3 and J'_3 are inequivalent, the two couplings may be different. Numbers from 0 to 3 label the four fcc sublattices.

pyrochlore lattice with interactions going beyond nearest neighbors. Following up on previous works by Reimers *et al.*¹² and by Tsuneishi *et al.*¹³, we consider the classical Heisenberg antiferromagnet on the pyrochlore lattice with the Hamiltonian

$$\mathcal{H} = J_1 \sum_{\langle ij \rangle} \mathbf{S}_i \cdot \mathbf{S}_j + J_2 \sum_{\langle\langle ij \rangle\rangle} \mathbf{S}_i \cdot \mathbf{S}_j, \quad (1)$$

where $\langle ij \rangle$ and $\langle\langle ij \rangle\rangle$ indicate pairs of first and second neighbors, respectively. Given the short-range nature of exchange forces, we work in the limit $J_2 \ll J_1$. It is reasonable to expect that the influence of J_2 becomes noticeable only at low temperatures of order $J_2 S^2$, when the system is already in the strongly correlated paramagnetic state, in which it is constrained to fluctuate around the ground states of the nearest neighbor exchange. Using a combination of Monte Carlo simulations and analytical arguments, we have mapped out the phase diagram in

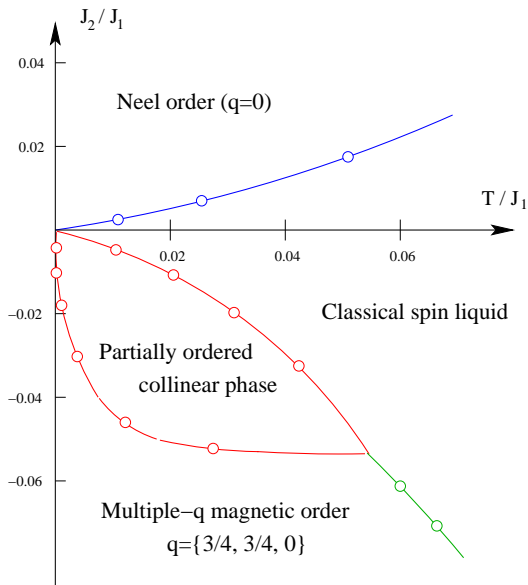


FIG. 2: Phase diagram of the model with antiferromagnetic first and weak second-neighbor exchange of either sign on the pyrochlore lattice. Open circles denote locations of thermodynamic phase transitions (all first order), lines are interpolated phase boundaries.

the J_2 - T plane shown in Fig. 2.

Antiferromagnetic second-neighbor exchange, $J_2 > 0$, significantly reduces the frustration by selecting states in which spins within any of the four fcc sublattices, comprising the pyrochlore lattice, are parallel to one another. We find a collinearly ordered phase of the type $\langle \mathbf{S}_0 \rangle = \langle \mathbf{S}_1 \rangle = -\langle \mathbf{S}_2 \rangle = -\langle \mathbf{S}_3 \rangle$, where the subscripts enumerate the fcc sublattices (Fig. 1). The transition between the paramagnetic and antiferromagnetic phases is discontinuous.

Ferromagnetic second-neighbor exchange, $J_2 < 0$, leaves the system strongly frustrated. A mean-field calculation by Reimers *et al.*¹² predicted a ground state with incommensurate magnetic order. While Tsuneishi *et al.*¹³ indeed observed Bragg peaks in the spin structure factor obtained through a Monte Carlo simulation for $J_2 = -0.1J_1$, they also noted that the spins remained dynamic, failing to freeze. We show that the observed locations of the Bragg peaks are compatible with the results of Reimers *et al.*, so that the low-temperature phase is most likely magnetically ordered.

The main focus of our paper is a peculiar *partially ordered* phase sandwiched between the paramagnet and the magnetically ordered state for weak enough ferromagnetic J_2 , namely $-0.05J_1 \lesssim J_2 < 0$. In the intermediate phase, the spins display collinear order; furthermore, they exhibit magnetic order within a thin $\{100\}$ layer but no order across different layers. The partial order can be characterized by a combination of a director $\hat{\mathbf{n}}$ specifying a global spin axis, a Potts (Z_3) variable $q = (100)$, (010) , or (001) specifying the direction of the layers, and an Ising (Z_2) variable σ_n for *each layer* identifying one

of the two possible spin orientations within a layer. The order is partial in the sense that the Ising variables $\{\sigma_n\}$ randomly pick values of $+1$ and -1 with no discernible correlations between adjacent layers. The partially ordered state is bounded by first-order transitions on both the high-temperature side, $T_{c1} = \mathcal{O}(J_2)$, and the low-temperature side, $T_{c2} = \mathcal{O}(J_2^2/J_1)$.

Similar partial order has been previously found in a $1/S$ treatment of the Heisenberg antiferromagnet on the checkerboard lattice, also known as the square lattice with crossings, a two-dimensional analog of the pyrochlore.¹⁴ In both systems the distinct layered states are *not* related to one another by a symmetry of the Hamiltonian and simply arise as different local minima of the free energy. Free-energy barriers separating them scale as a power of the system size, so that the system will not be ergodic in the thermodynamic limit and instead will remain in one of these minima forever.

While we have focused on the role of second-neighbor exchange J_2 in the formation of magnetic order on the pyrochlore lattice, our results also shed light on the role of third-neighbor interactions J_3 (see Fig. 1). In view of strong correlations between nearest-neighbor spins developing at temperatures well below $J_1 S^2$, the second and third-neighbor exchanges are no longer independent coupling constants. Indeed, the relative shift in energy for any pair of ground states of the nearest-neighbor exchange due to a small J_3 is identical to the effect of a J_2 of the same magnitude and opposite sign. Thus our findings should also be of relevance for the more general case of a pyrochlore antiferromagnet with small J_2 and J_3 .

The remainder of this paper is organized as follows. In Sec. II we briefly discuss the nature of magnetically ordered phases at low temperatures for both signs of the second-neighbor coupling J_2 . Sec. III presents the main subject of this work, the partially ordered phase found at intermediate temperatures on the ferromagnetic side of J_2 . Stability of the partially ordered state and its phase boundaries are examined in Sec. IV. We conclude with a discussion of these results in Sec. V.

II. LOW-TEMPERATURE ORDERED PHASES

A. Antiferromagnetic J_2 : low frustration

In the limit $J_2 \ll J_1$, magnetic ordering takes place at a temperature $T_c = \mathcal{O}(J_2 S^2)$. The nature of this ordering is best understood by appealing to the fact that a weak third-neighbor coupling $J_3 \ll J_1$ (Fig. 1) selects among the nearest-neighbour ground states in the same way as a second-neighbor coupling J_2 of the same strength and opposite sign, as explained in Appendix A. (We here note in passing that, since the strength of coupling depends on the exchange paths and not the interatomic distance alone, sometimes J_3 may be as big as J_2 . For instance, *ab initio* calculations show that in CdCr_2O_4 J_3 exceeds J_2

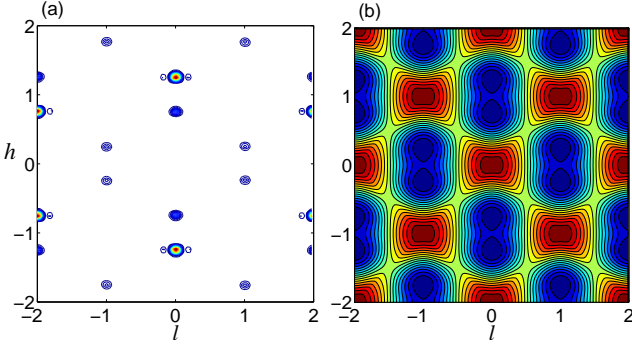


FIG. 3: (a) The spin structure factor of the Neel state at wavevectors $\mathbf{q} = 2\pi(h, h, l)$. (b) Minimum eigenvalue of the exchange matrix $J_{mn}(\mathbf{q})$ at wavevectors $\mathbf{q} = 2\pi(h, h, l)$ for $J_2 = -J_1/10$. The satellite peaks might be due to the finite-size effect for an incommensurate spin order.

in magnitude.^{15,16}) This insight is useful as the resulting ordered pattern can be understood in a more straightforward way by analyzing the effect of J_3 . To see that, note that the pyrochlore lattice consists of four fcc sublattices and that third neighbors on the pyrochlore lattice belong to the same fcc sublattice (Fig. 1). Thus a ferromagnetic exchange $J_3 < 0$ is not frustrated and will be absolutely minimized by a state where spins within the same fcc sublattice are parallel to one another.

A translationally invariant four-sublattice ground state was predicted for the pyrochlore antiferromagnet with a ferromagnetic J_3 by Reimers *et al.*¹² The same can be expected for an antiferromagnetic second-neighbor coupling $J_2 > 0$.

Using Monte Carlo simulations, the $\mathbf{q} = 0$ Néel state with up-up-down-down spin configuration on every tetrahedron is indeed found to be the ground state for an antiferromagnetic J_2 . This collinear magnetic state is separated by a discontinuous transition line from the high-temperature cooperative paramagnetic state (Fig. 2).

B. Ferromagnetic J_2 : high frustration

The case of a ferromagnetic second-neighbor coupling, $J_2 < 0$, is similar to that of $J_3 > 0$. An antiferromagnetic coupling on an fcc lattice is frustrated, so that this time one may expect a more complex magnetic order. Indeed, Reimers's mean-field calculation yields an incommensurate magnetic order with a wavevector $\mathbf{q} = (h, h, 0)$ in the case of a ferromagnetic J_2 .

We performed Monte Carlo simulations on the pyrochlore lattice with periodic boundary conditions measuring 8 cubic unit cells in each direction. The simulations were done for $J_2 = -0.1 J_1$. They revealed a state with magnetic Bragg peaks at incommensurate lattice momenta near $2\pi\{3/4, 3/4, 0\}$ and other equivalent positions. Fig. 3(a) shows two inequivalent Bragg peaks, $2\pi(3/4, 3/4, 0)$ and $-2\pi(3/4, 3/4, 0)$, the rest being re-

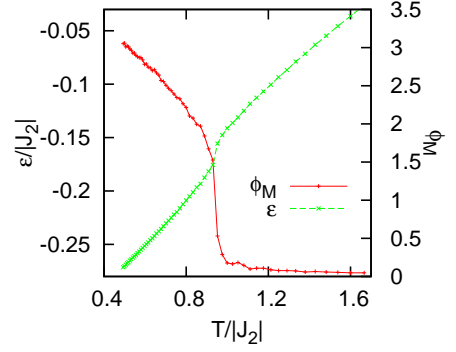


FIG. 4: The phase transition between the paramagnetic and antiferromagnetic phases for $J_2 = -0.1J_1$. The normalized energy density $\varepsilon = (E - E_0)/6N$, where $E_0 = -NJ_1$ is the ground state energy of nearest-neighbor interactions. ϕ_M is the second moment of the magnetic order parameters.

lated to these two by a reciprocal lattice vector. Bragg peaks with comparable intensities are found at other wavevectors related to the above two by point-group symmetries. This multiple- \mathbf{q} Néel order is consistent with the ground states of (1) in the spherical approximation, in which the local unit-length constraints $|\mathbf{S}_i| = 1$ are replaced by a global one $\sum_{i=1}^N |\mathbf{S}_i|^2 = N$. Introducing the Fourier transform $\mathbf{S}_i = \sum_{\mathbf{q}} \mathbf{S}_m(\mathbf{q}) e^{i\mathbf{q} \cdot \mathbf{r}_i}$ (the site index $i = (m, \mathbf{r}_i)$, where m is the sublattice index), the exchange interaction (1) becomes

$$\mathcal{H} = \frac{N}{4} \sum_{\mathbf{q}} \sum_{m,n=0}^3 J_{mn}(\mathbf{q}) \mathbf{S}_m(\mathbf{q}) \cdot \mathbf{S}_n(-\mathbf{q}). \quad (2)$$

The Fourier components $\mathbf{S}_m(\mathbf{q})$ are subject only to a global constraint $\sum_{m,\mathbf{q}} |\mathbf{S}_m(\mathbf{q})|^2 = 1$. The matrix $J_{mn}(\mathbf{q})$ is the Fourier transform of exchange interaction J_{ij} . Its explicit form with interactions up to the fourth neighbors can be found in Ref. 12.

Expanding $\mathbf{S}_m(\mathbf{q}) = \sum_a U_{\mathbf{q},m}^a \Phi_{\mathbf{q}}^a$ in terms of the eigenvectors $U_{\mathbf{q},m}^a$ of the exchange matrix $J_{mn}(\mathbf{q})$ yields the energy as a function of the expansion coefficients $\Phi_{\mathbf{q}}^a$:

$$E = \frac{N}{4} \sum_{\mathbf{q}} \sum_{a=1}^4 \lambda_{\mathbf{q}}^a |\Phi_{\mathbf{q}}^a|^2, \quad (3)$$

where $\lambda_{\mathbf{q}}^a$ is the corresponding eigenvalue of $J_{mn}(\mathbf{q})$. With the normalization $\sum_{m=0}^3 |U_{\mathbf{q},m}^a|^2 = 1$, the vectors $\Phi_{\mathbf{q}}^a$ satisfy $\sum_{\mathbf{q}} \sum_a |\Phi_{\mathbf{q}}^a|^2 = 1$. The ground state energy of (2) is thus $E_0 = N\lambda_{\min}$, where λ_{\min} is the lowest eigenvalue $\lambda_{\mathbf{q}}^a$.

For the nearest-neighbor interaction only, the two lowest eigenvalues are \mathbf{q} -independent, $\lambda_{\mathbf{q}}^1 = \lambda_{\mathbf{q}}^2 = -J_1$, reflecting the degenerate nature of the magnetically ordered ground state. This degeneracy is lifted by the introduction of J_2 as discussed by Reimers *et al.*¹² A contour plot of the lowest eigenvalue of the exchange matrix as

a function of the wavevector $\mathbf{q} = 2\pi(h, h, l)$ for $J_2 < 0$ is shown in Fig. 3(b). It can be seen from Fig. 3 that the peaks of the spin structure factor appear at the same locations as the minima of exchange energy, namely at 12 incommensurate wavevectors $\mathbf{q}^* = 2\pi\{h^*, h^*, 0\}$, where $h^* \approx 3/4$ depends weakly on the ratio J_2/J_1 . For small J_2/J_1 , $h^* = a_0 + a_1(J_2/J_1) + \mathcal{O}((J_2/J_1)^2)$, where

$$\begin{aligned} a_0 &= \frac{1}{\pi} \arccos[(4\sqrt{3} - 9)/3] = 0.7427, \\ a_1 &= \frac{44}{3\pi\sqrt{9654 + 5574\sqrt{3}}} = 0.0336. \end{aligned} \quad (4)$$

The magnetic order is described by the order parameter composed of 12 vector amplitudes $\Phi_{\mathbf{q}^*}$.¹² A detailed characterization of this magnetic state is deferred to a future publication. Fig. 4 shows the temperature dependence of the energy density ε and the magnitude of the order parameters $\phi_M = \sum_{\mathbf{q}^*} |\Phi_{\mathbf{q}^*}|^2$. Both exhibit a clear jump at $T_c \approx 0.95|J_2|$, indicating a first-order transition. This is also confirmed by a double-peak structure in the energy histogram at the transition temperature. Similar results were obtained for $J_2 \lesssim -0.05 J_1$ where the magnetic phase is separated from the high-temperature spin liquid phase by a first-order phase transition as indicated in Fig. 2.

III. PARTIALLY ORDERED PHASE

As discussed in the Introduction, an intermediate phase with collinear spins exists at finite temperatures for a small ferromagnetic coupling $J_2 < 0$. The appearance of collinearity is not totally unexpected as it is well known that collinear states are in general favored by thermal fluctuations in magnets with frustrated exchange interactions.¹⁷ The fact that the system remains frustrated even in the presence of a ferromagnetic J_2 makes the existence of the nematic phase possible. From another perspective, the classical nearest-neighbor Heisenberg spins on the pyrochlore lattice evade the thermal selection only marginally.⁵ The introduction of a ferromagnetic J_2 reduces the dimension of ground-state manifold, thus permitting thermal fluctuations to stabilize collinear states.

A. Nematic order

To demonstrate that spins indeed become collinear in the intermediate phase, we have obtained from Monte Carlo simulations the nematic order parameter Q defined as the largest eigenvalue of the traceless tensor $Q_{\mu\nu} = \langle S_\mu S_\nu - \delta_{\mu\nu}/3 \rangle$,¹⁸ where S_μ represents Cartesian components of a spin. It vanishes in a totally disordered state and attains the maximal value of $2/3$ for parallel spins.

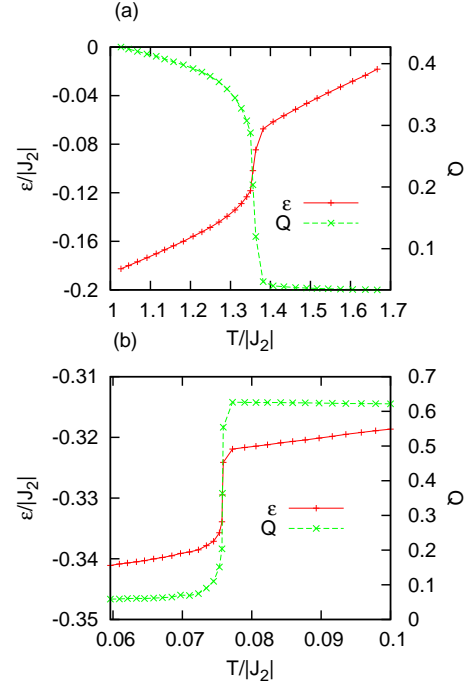


FIG. 5: Transitions between (a) the paramagnetic and nematic phases, and (b) the nematic and Néel phases, for $J_2 = -0.01J_1$. The normalized energy density $\varepsilon = (E - E_0)/6N$, where $E_0 = -NJ_1$ is the ground state energy of nearest-neighbor interactions. Q is the spin nematic order parameter.

The thermodynamic behavior of the system with $J_2 = -0.01 J_1$ in the vicinity of the phase transitions is illustrated in Fig. 5. The simulation was done on the pyrochlore lattice with periodic boundary conditions measuring 4 cubic unit cells in each direction, giving a total of $N = 16 \times 4^3 = 1024$ spins. To improve the equilibration process, we employed parallel tempering^{19,20} with 30 replicas. The energy density ε and the nematic order parameter Q are shown as functions of temperature near T_{c1} [paramagnet to partially ordered phase, Fig. 5 (a)] and T_{c2} [partially ordered phase to antiferromagnet, Fig. 5 (b)]. The energy density shows a clear discontinuity at both transitions. Extrapolating the energy curve from the partially ordered phase to $T = 0$ yields a density $\varepsilon_L = -|J_2|/3$ characteristic of a layered state to be discussed below. Likewise, the order parameter Q extrapolates to the maximal attainable value of $2/3$ characteristic of collinear spins. Below T_{c2} , the antiferromagnetic state seems to have a residual nematic order with $Q \approx 0.05$, which may be intrinsic to the low-temperature ordered state, or a finite-size effect.

B. Bond order

Nematic order alone does not provide a full characterization of this phase: four spins on a tetrahedron have three distinct collinear states not related to each other by a global rotation of the spins. They are labeled red,

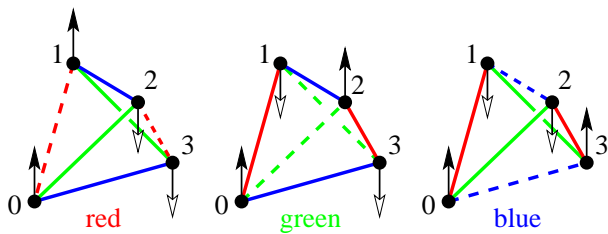


FIG. 6: The three distinct collinear states of a tetrahedron. Frustrated bonds (with parallel spins) are shown as dashed lines.

green, and blue in Fig. 6. These states differ from one another by the location of frustrated bonds $\langle ij \rangle$ that involve parallel spins. Since the global direction of the spins is already captured by the nematic order parameter $Q_{\mu\nu}$, further characterization can be made by using scalar quantities, such as bond variables $f_{ij} \equiv \langle \mathbf{S}_i \cdot \mathbf{S}_j \rangle$. At temperatures well below $J_1 S^2$ only two (out of six) bond variables of a tetrahedron are independent:⁹

$$\begin{aligned} f_1 &= \frac{f_{01} + f_{23} + f_{02} + f_{13} - 2f_{03} - 2f_{12}}{\sqrt{12}}, \\ f_2 &= \frac{f_{01} + f_{23} - f_{02} - f_{13}}{2}. \end{aligned} \quad (5)$$

The vector $\mathbf{f} = (f_1, f_2)$ takes on values in a triangular domain with the three collinear states in its corners.

What kind of bond order might one expect in the intermediate phase? To answer this question, let us again use the equivalence between a ferromagnetic J_2 and an antiferromagnetic J_3 . The latter promotes antiparallel orientations for spins 3 and 3' (Fig. 1), which means—for a collinear state of spins—that one of the bonds 03 and 03' is frustrated and the other is satisfied. (Bergman *et al.*²¹ showed that such states—satisfying the “bending rule” for frustrated bonds in zero applied field—are also favored by quantum fluctuations of spins.) In other words, adjacent tetrahedra will be in states of different color. This is reminiscent of the antiferromagnetic Potts model with 3 states: red, green and blue in Fig. 6. A collinear state of the pyrochlore antiferromagnet is fully specified by the global spin director and the colors of all tetrahedra. Note however that colors of tetrahedra are not completely independent: the number of satisfied bonds ($\mathbf{S}_i \cdot \mathbf{S}_j = -S^2$) must be even along any closed loop. Nonetheless, the parametrization in terms of Potts variables serves a useful purpose. One of the phases of the antiferromagnetic Potts model on a bipartite lattice has a broken sublattice symmetry (BSS): one sublattice is dominated by one color, while the other is randomly populated by the two remaining colors.^{22,23} With this state in mind, we have measured the average bond variables in the intermediate phase in the Monte Carlo simulations.

The Monte Carlo averages of the bond doublet (5) for sublattices *A* and *B* are shown in Fig. 7. The value of \mathbf{f} for sublattice *A* is narrowly distributed in the vicinity of the collinear blue state, indicating that all tetrahe-

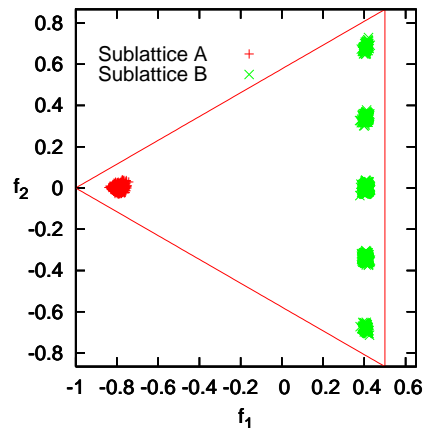


FIG. 7: Histogram of bond vector of the two sublattices \mathbf{f}_A and \mathbf{f}_B in the nematic phase. The bond vector \mathbf{f} has been normalized such that the three collinear states are at vertices $(-1, 0)$, $(1/2, \sqrt{3}/2)$, and $(1/2, -\sqrt{3}/2)$.

dra of sublattice *A* are in this state. There are no blue tetrahedra on sublattice *B*, as one might expect from the analogy with the antiferromagnetic Potts model. For the BSS phase, where each site is red or green with equal probabilities, one expects a continuous distribution of \mathbf{f} in the middle of the opposing edge of the triangle connecting the green and red corners. Instead, we find that sublattice *B* has discrete fractions of red tetrahedra: 0, 1/4, 1/2, 3/4, and 1.

This discreteness is a finite-size effect: an examination of individual microstates shows that the intermediate phase has a layered structure for bond variables on sublattice *B*: tetrahedra within the same layer in the *xy* plane have the same color. The origin of the layered structure on one of the sublattices can be traced to the same constraint on the colors around a closed loop. See Appendix B for details. Our finite system contained 8 layers of tetrahedra within a sublattice. If the layers could be colored red and green independently of one another, one would expect to find the fractions of either color proportional to 1/8. However, periodic boundary conditions create constraints on the number of satisfied bonds in the direction perpendicular to the layers, so that each lattice can only have an even number of layers of either color. Hence the fractions proportional to 1/4.

To verify this observation more directly, we performed a replica-exchange Monte Carlo simulation on a system with 4^3 conventional cubic cells. 16×4^3 spins are divided into 8 layers of tetrahedra in each sublattice. A particular layered state with collinear spins is described by a sequence of Ising variables $\{\sigma_1, \sigma_2, \dots, \sigma_8\}$ (see Appendix C). With periodic boundary conditions, 17 distinct configurations are used in a replica-exchange Monte Carlo simulation. The Ising sequences corresponding to these 17 layered states are listed in Table I. In each exchange cycle, a fixed number of Metropolis sweeps are performed on individual replicas of the system, each of which corre-

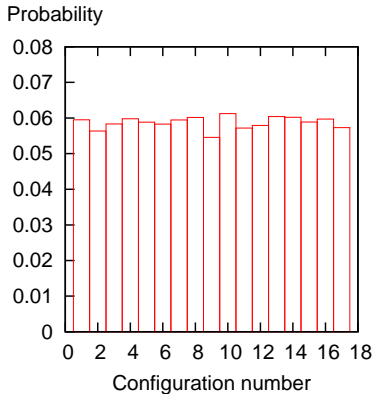


FIG. 8: Histogram of 17 distinct collinear layered structures obtained by replica-exchange Monte Carlo simulation. The system has 16×4^3 spins. The configuration number labels 17 topologically distinct layered states subject to the periodic boundary condition.

sponds to a particular layered state. Then different replicas are exchanged according to detailed balance, thus ensuring thermodynamic equilibrium. A histogram of the occurrence of the 17 configurations in a chosen replica is shown in Fig. 8. The almost equal probability of occurrence implies a vanishing spin order after averaging over the different configurations.

The layered structure of the intermediate phase spontaneously breaks the rotational and translational symmetries of the pyrochlore lattice. A collinear Néel order exists within an individual layer of tetrahedra but not across the layers if the colors on one sublattice are indeed random. At the mean-field level, the layered collinear states belong to a larger class of (generally non-collinear) layered states with the same exchange energy. A discussion of the general layered states can be found in Appendix C.

IV. STABILITY OF THE PARTIALLY ORDERED PHASE

A. Unstable modes

To analyze the stability of a collinear state, we express the energy of the system in terms of transverse spin fluctuations $\boldsymbol{\sigma}_i \perp \hat{\mathbf{n}}$. By substituting $\mathbf{S}_i \approx (1 - \sigma_i^2/2)\eta_i \hat{\mathbf{n}} + \boldsymbol{\sigma}_i$ into Eq. (1) we obtain a spin-wave Hamiltonian in the harmonic approximation,

$$\mathcal{H}^{(2)} = E_L + (J_1 - 2J_2) \sum_i \sigma_i^2 + \frac{1}{2} \sum_{i,j} J_{ij} \boldsymbol{\sigma}_i \cdot \boldsymbol{\sigma}_j, \quad (6)$$

where E_L is the energy of the layered state. The Ising variables $\{\eta_i\}$ specifying the direction of a spin are absent from the harmonic Hamiltonian (6). They affect the dynamics of the system through the canonical commutation relations for the transverse components of the spins.

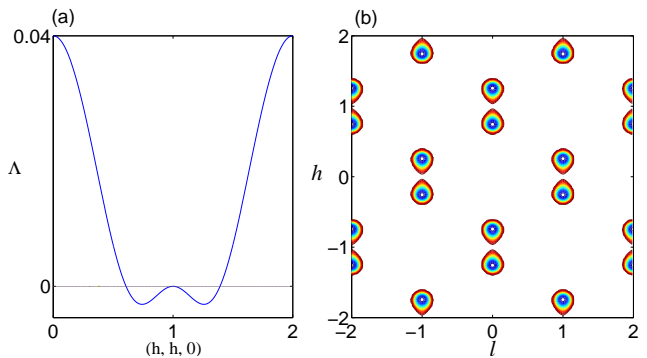


FIG. 9: (a) The energy dispersion of the spin-wave band with unstable modes. (b) Regions in momentum space $\mathbf{q} = 2\pi(h, h, l)$ where the spectrum of energy fluctuations has negative eigenvalues $\Lambda_{\mathbf{q}}^a$. $J_1 = 1$, $J_2 = -0.1$.

The quadratic form (6) must be positive definite to guarantee stability of the collinear state. Its eigenvalues Λ are obtained by making the Fourier transform and then diagonalizing a 4×4 matrix (the pyrochlore lattice is an fcc with a basis of 4 sites):

$$\Lambda_{\mathbf{q}}^a = (J_1 - 2J_2) + \lambda_{\mathbf{q}}^a, \quad (7)$$

where $\lambda_{\mathbf{q}}^a$ are eigenvalues of $J_{mn}(\mathbf{q})$ defined in Sec. II B. The dispersion has degenerate zero modes along lines $\mathbf{q} = 2\pi\{1, h, 0\}$ corresponding to magnetic spirals along one of the three cubic axes. These spirals belong to the degenerate manifold of non-collinear layered states discussed in Appendix C. Furthermore, there are regions in momentum space with $\Lambda_{\mathbf{q}} < 0$, as shown in Fig. 9. The most unstable modes are found at wavevectors $\mathbf{q} = 2\pi\{h^*, h^*, 0\}$ with h^* given by Eq. (4). For small J_2/J_1 , the lowest eigenvalue is

$$\Lambda_{\min} = (30 - 16\sqrt{3}) \frac{J_2}{J_1} + \frac{32}{3} (56\sqrt{3} - 97) \left(\frac{J_2}{J_1} \right)^2 + \dots$$

Since $\Lambda_{\min} < 0$ for a ferromagnetic J_2 , the collinear ground states are unstable at zero temperature.

B. Hartree-Fock calculation

At finite temperatures the collinear layered states are stabilized by thermal fluctuations. To demonstrate this, we go beyond the harmonic term of the classical Holstein-Primakoff expansion and consider the interactions between spin waves,²⁴

$$\mathcal{H}^{(4)} = \frac{1}{8} \sum_{i,j} J_{ij} \left[\eta_i \eta_j \sigma_i^2 \sigma_j^2 - \frac{1}{2} \boldsymbol{\sigma}_i \cdot \boldsymbol{\sigma}_j (\sigma_i^2 + \sigma_j^2) \right]. \quad (8)$$

Since the system is unstable at the harmonic order, a perturbation expansion based on the quadratic Hamiltonian (6) is not possible. Instead, following Hizi and Henley,²⁴

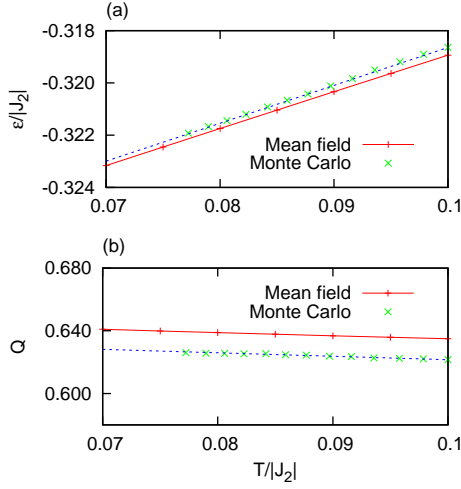


FIG. 10: (a) energy density ε and (b) nematic order parameter as a function of temperature obtained using Monte Carlo simulations and a Hartree-Fock self-consistent calculation. The calculation was done with $J_2 = -0.01J_1$. The dashed line is a linear fit to the Monte Carlo data. Note that the transition temperature obtained from Monte Carlo simulation is $T_{c2} \approx 0.076|J_2|$.

we construct an effective (mean-field) quadratic Hamiltonian $\mathcal{H}_{\text{MF}} = \sum_{i,j} \tilde{H}_{ij}^{(2)} \sigma_i \cdot \sigma_j$ that provides the best approximation to $\mathcal{H}^{(2)} + \mathcal{H}^{(4)}$. Its coefficients $\tilde{H}_{ij}^{(2)}$ read

$$(J_1 - 2J_2) + \frac{1}{2} \sum_k J_{ik} (\eta_i \eta_k G_{kk} - G_{ik}) \quad (i = j),$$

$$\frac{1}{2} J_{ij} \left[1 + \eta_i \eta_j G_{ij} - \frac{1}{2} (G_{ii} + G_{jj}) \right] \quad (i \neq j). \quad (9)$$

Here $G_{ij} = \langle \sigma_i^x \sigma_j^x \rangle = \langle \sigma_i^y \sigma_j^y \rangle$ is the correlation function of spin fluctuations calculated self-consistently in the thermal ensemble of the mean-field Hamiltonian (9)

$$G_{ij} = \frac{\int D\sigma \sigma_i^x \sigma_j^x e^{-\beta \mathcal{H}_{\text{MF}}}}{\int D\sigma e^{-\beta \mathcal{H}_{\text{MF}}}}. \quad (10)$$

Numerically, an iteration process is used to obtain the correlation functions G_{ij} . After self-consistency is reached, the energy of the magnet is given by

$$E_{\text{MF}} = E_L + 2 \sum_i (J_1 - 2J_2) G_{ii} + \sum_{i,j} J_{ij} G_{ij} \quad (11)$$

$$+ \frac{1}{2} \sum_{i,j} J_{ij} \left[\eta_i \eta_j (G_{ii} G_{jj} + G_{ij}^2) - G_{ij} (G_{ii} + G_{jj}) \right].$$

Fig. 10 (a) shows the computed energy density as a function of temperature. The result agrees very well with that obtained from Monte Carlo simulations. Both the simulation and calculation were done for $J_2 = -0.01J_1$ on a pyrochlore lattice with a size of 16×4^3 spins and periodic boundary condition on each side. The self-consistent method can also be used to compute the nematic order parameter. For $\hat{\mathbf{n}} = +\hat{\mathbf{z}}$, the tensor $\langle S_\mu S_\nu \rangle$ becomes diagonal with elements $\langle S_x S_x \rangle = \langle S_y S_y \rangle = 2\bar{G}$ and

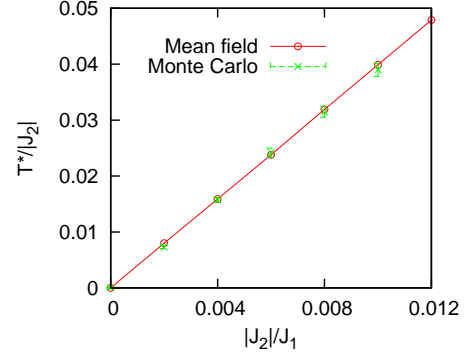


FIG. 11: Stability boundary T^* obtained using Hartree-Fock calculation and Monte Carlo simulations. The errorbars associated with the Monte Carlo data is the temperature step ΔT used in the simulation.

$\langle S_z S_z \rangle = 1 - 2\bar{G}$, where $\bar{G} = \sum_i G_{ii}/N$. The nematic order parameter is then

$$Q = \frac{2}{3} - \frac{2}{N} \sum_i G_{ii}. \quad (12)$$

The result is shown in Fig. 10 (b) and the agreement with that obtained from Monte Carlo simulation seems satisfactory. The nearly saturated nematic order parameter Q observed in Monte Carlo simulations implies $\sigma^2 \ll 1$, justifying the Holstein-Primakoff expansion about the collinear state.

Below a certain temperature T^* the energy spectrum of spin waves acquires some negative eigenvalues and the collinear phase gives way to the low-temperature ordered state. Since the transition is first order, the $E - T$ diagram exhibits hysteresis. The thermodynamic transition takes place at a temperature $T_{c2} > T^*$, at which the collinear phase is still locally stable.

The dependence of $T^*/|J_2|$ on the ratio $|J_2|/J_1$ obtained from the Hartree-Fock calculation is shown in Fig. 11. The points collapse perfectly on a linear curve implying a scaling relation $T^* \sim J_2^2/J_1$. A numerical estimate of the stability boundary $T^*(J_2)$, obtained as the lowest temperature at which the intermediate phase was still observed in Monte Carlo runs, is also plotted in Fig. 11; the result is in satisfactory agreement with that of the mean-field calculation.

C. Analytic results: red-and-green state

An analytical derivation of the stability temperature $T^* \sim J_2^2/J_1$ is difficult to obtain for the most general layered state. We have evaluated the stability for the simplest state of this kind, where all of the layers have the same colors. A state of this sort (sublattice A is red and sublattice B is green) was studied in Ref. 15. This particular state has a higher symmetry than a typical layered structure: the color variables violate only

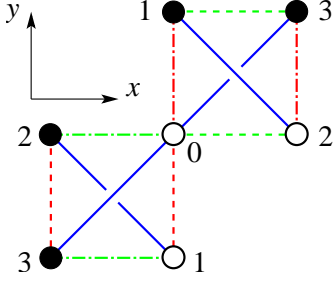


FIG. 12: Renormalized nearest neighbor bonds of the red-and-green state in the mean-field calculation. The renormalized first-neighbor exchange constants: $J_1 - K_1 - K_2$ (dashed bonds), $J_1 - K_1$ (dash-dotted bonds), and $J_1 - K_2$ (solid bonds).

the inversion symmetry exchanging the two sublattices of tetrahedra.

In the mean-field Hamiltonian (9), the main effects of the quartic interaction $\mathcal{H}^{(4)}$ is to renormalize the first-neighbor exchange J_1 to $J_{ij} = J_1 + \delta J_{ij}$, which is now bond-dependent:

$$\delta J_{ij} = -\frac{J_1}{2}(G_{ii} + G_{jj} - 2\eta_i\eta_j G_{ij}). \quad (13)$$

Assuming that exchange renormalizations δJ_{ij} respect the symmetries of the red-and-green state, we have 3 independent variational parameters δJ_{01} , δJ_{02} , and δJ_{03} (Fig. 12). If we further assume that the correlations G_{ij} are dominated by the pyrochlore zero modes, the number of variational parameters reduces to 2. This is so because zero modes satisfy $\sum_{i=0}^3 \sigma_i = 0$, hence $\langle \sigma_0 \sigma_1 \rangle = -\langle \sigma_0^2 \rangle - \langle \sigma_0 \sigma_2 \rangle - \langle \sigma_0 \sigma_3 \rangle$. It follows then that $\delta J_{01} = \delta J_{02} + \delta J_{03}$. We parametrize the exchange renormalizations in terms of K_1 and K_2 such that

$$\begin{aligned} \delta J_{01} &= \delta J_{23} = -K_1 - K_2, \\ \delta J_{02} &= \delta J_{31} = -K_1, \\ \delta J_{03} &= \delta J_{12} = -K_2 \end{aligned} \quad (14)$$

on the red sublattice.

We then compute the spectrum and the eigenmodes of energy fluctuations with the renormalized exchange interaction. The two zero-energy bands that were flat in the absence of J_2 and K_i now acquire a dispersion; one becomes gapped ($\Lambda_{\mathbf{q}}^a$ is strictly positive), while the other has a vanishing energy at the wavevector $\mathbf{q}_0 = 2\pi(0, 0, 1)$. This zero mode corresponds to a global rotation of spins. Correlation functions are dominated by fluctuations in the lowest band in the vicinity of \mathbf{q}_0 . For small \mathbf{k} , the energy eigenvalue is

$$\Lambda_{\mathbf{q}_0+\mathbf{k}} \approx \frac{1}{32} [2K_1 k_{\perp}^2 + (8|J_2| + K_2)k_z^2], \quad (15)$$

where $k_{\perp}^2 = k_x^2 + k_y^2$.

In order to obtain the correlations G_{ij} , we need first to obtain the eigenmodes. To this end, we use an orthonormal basis of the two zero modes of J_1 for given values of

\mathbf{k} . We then treat K_i and J_2 as perturbations and use degenerate perturbation theory to obtain the eigenmodes. To the lowest order in \mathbf{k} the eigenmodes are

$$\begin{aligned} u_0(\mathbf{q}_0 + \mathbf{k}) &= -i/2 - (k_x - k_y + k_z)/16, \\ u_1(\mathbf{q}_0 + \mathbf{k}) &= +1/2 - i(k_x + k_y + k_z)/16, \\ u_2(\mathbf{q}_0 + \mathbf{k}) &= -1/2 - i(k_x + k_y - k_z)/16, \\ u_3(\mathbf{q}_0 + \mathbf{k}) &= +i/2 - (k_x - k_y - k_z)/16. \end{aligned} \quad (16)$$

As can be easily checked, the total spin of a tetrahedron $\sum_m \sigma_m = \sum_m u_m e^{i(\mathbf{q}_0+\mathbf{k})\cdot\mathbf{r}_m} = 0$ at this order in k . The spin correlation function is

$$G_{mn} = \frac{1}{N'} \sum_{\mathbf{q}} \frac{T}{\Lambda_{\mathbf{q}}} u_m^*(\mathbf{q}) u_n(\mathbf{q}) e^{i(\mathbf{q})\cdot(\mathbf{r}_m - \mathbf{r}_n)}, \quad (17)$$

where $N' = N/4$ is the number of unit cells, and m, n are sublattice indices. By expanding to the second order of k and using (13), we obtain the following self-consistency equations for K_1 and K_2

$$\frac{J_1 T}{4N'} \sum_{\mathbf{k}} \frac{k_z^2}{2K_1 k_{\perp}^2 + (8|J_2| + K_2)k_z^2} = K_1, \quad (18)$$

$$\frac{J_1 T}{2N'} \sum_{\mathbf{k}} \frac{k_{\perp}^2}{2K_1 k_{\perp}^2 + (8|J_2| + K_2)k_z^2} = K_2, \quad (19)$$

Although these equations can be solved numerically, we are interested in an approximate solution of K_1 and K_2 in the low-temperature regime, $T \ll |J_2|$. Since the effective spin stiffness K is generated by thermal fluctuations, they are expected to be small compared to J_2 . To the lowest order we neglect K_1 and K_2 in Eq. (18) and obtain

$$K_1 \approx \frac{J_1 T}{32|J_2|}. \quad (20)$$

On the other hand, because the integral for K_2 is divergent as $K_1 \rightarrow 0$, we must keep K_1 in Eq. (19). Substituting the result for K_1 into Eq. (19), we obtain

$$K_2 \approx \frac{\pi}{3\sqrt{2}} \sqrt{J_1 T} \quad (21)$$

to the lowest order in T .

These results provide a glimpse into the physics of the transition between the intermediate and low-temperature phases. Fig. 13 shows the renormalized dispersion $\Lambda_{\mathbf{q}_0+\mathbf{k}}$ (15) along the line $\mathbf{q} = 2\pi(h, h, 1)$ at various temperatures. As the temperature decreases, a dip of the dispersion curve starts to develop at $h \approx 0.2$. Eventually this local minimum touches zero at the critical temperature T_{c2} ; below T^* the collinear state is unstable: it decays by emitting spin waves with $\mathbf{q} \approx 2\pi(1/4, 1/4, 1)$. The picture is consistent with the first-order transition observed in the Monte Carlo simulations.

It should be noted that the scenario displayed in Fig. 13 is only a qualitative description of the real phase transition. Our self-consistent treatment only takes into account spin waves close to the $\mathbf{q}_0 = 2\pi(0, 0, 1)$ Goldstone

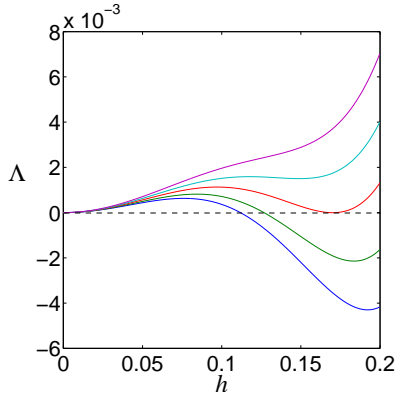


FIG. 13: Variation of spin-wave energy Λ in unit of $|J_2|$ along the $\mathbf{q} = 2\pi(h, h, 1)$ line. The calculation was done with a $J_2 = -0.01J_1$. The curves correspond to temperatures $T/|J_2| = 0.018, 0.0165, 0.01526, 0.0145, 0.013$ (from top to bottom) with critical temperature $T_{c2} = 0.01526|J_2|$.

mode. This is valid at temperatures well above T^* since these spin waves are the lowest-energy excitations of the magnet. However, as $T \rightarrow T_{c2}$, spin waves with wavevectors $\mathbf{q} \approx 2\pi(1/4, 1/4, 1)$ become soft and should also be included in a self-consistent calculation. Additionally, we have studied the energy of spin waves as a proxy for the instability, whereas the proper calculation at a finite temperature should involve the free energy. We do this next.

D. Stability boundary: red-and-green state

We now provide an estimate of the stability temperature T^* by computing the magnon contribution to the system free energy. An expression (D9) for the change of free energy associated with an unstable mode is derived in Appendix D. Here we apply the result to the red-and-green state. We consider the most dangerous modes, namely those with wavevectors near $\mathbf{q}^* = 2\pi\{h^*, h^*, 1\}$ where $h^* \approx 1/4$. In the presence of such an unstable mode with amplitude ϕ superimposed on the red-and-green state, the free energy changes by an amount given by

$$\Delta F = \left(\Lambda^* + \sum_{mn} G_{mn} \Delta_{nm} \right) \phi^2, \quad (22)$$

where the correlation function G_{mn} is given by (17), and Δ_{mn} is the perturbation to the mean-field Hamiltonian \mathcal{H}_{MF} caused by the unstable mode. In our case, the real-space eigenvector of the unstable mode with $\mathbf{q}^* = 2\pi(h^*, h^*, 1)$ is

$$\mathbf{m}_n(\mathbf{r}) = U_n^* [\hat{\mathbf{x}} \cos(\mathbf{q}^* \cdot \mathbf{r}) + \hat{\mathbf{y}} \sin(\mathbf{q}^* \cdot \mathbf{r})], \quad (23)$$

where the corresponding momentum-space eigenvector for \mathbf{q}^* is

$$\mathbf{U}^* = (\cos \theta, -\sin \theta, -\sin \theta, \cos \theta) / \sqrt{2}, \quad (24)$$

with $\theta \approx 0.27\pi$ and weakly dependent on J_2 . We write the energy of the unstable mode as $\Lambda^* = -\gamma|J_2|$, where $\gamma \approx 0.2$ is a dimensionless number. The change of free energy is then

$$\Delta F / \phi^2 = -\gamma|J_2| + \frac{J_1 T}{4N'} \sum_{\mathbf{k}} \frac{\Delta_{\mathbf{k}}}{2K_1 k_{\perp}^2 + (8|J_2| + K_2)k_z^2}, \quad (25)$$

where

$$\Delta_{\mathbf{k}} = \sum_{m,n} \Delta_{mn} u_n^*(\mathbf{k}) u_m(\mathbf{k}) e^{i(\mathbf{q}_0 + \mathbf{k}) \cdot (\mathbf{r}_m - \mathbf{r}_n)}. \quad (26)$$

Since in most cases $\Delta_{\mathbf{k}} \sim \Delta + \mathcal{O}(k^2)$ for $h^* = 1/4$, we neglect the \mathbf{k} dependence of $\Delta_{\mathbf{k}}$ in the following as a lowest order approximation. With the aid of Eqs. (18) and (19), the integral evaluates to

$$\frac{\sqrt{2}\Delta}{16\pi} \sqrt{J_1 T}, \quad (27)$$

The condition $\Delta F = 0$ thus gives an estimate of the stability temperature

$$T^* = \left(\frac{16\pi\gamma}{\sqrt{2}\Delta} \right)^2 \frac{J_2^2}{J_1}. \quad (28)$$

This expression overestimates (by a factor of about 10) the stability temperature compared with numerical results. However, as mentioned previously, the discrepancy is due to the fact that we neglect contributions from the unstable modes themselves when approaching the transition temperature. Those modes with wavevector centered about the 12 unstable $\mathbf{q}^* = 2\pi\{h^*, h^*, 1\}$ become extremely soft as $T \rightarrow T^*$ and should be included in the calculation in a self-consistent way. Nevertheless, (28) provides an upper bound of the stability boundary and gives a scaling relation consistent with the numerical data.

V. DISCUSSION

We have studied the classical Heisenberg antiferromagnet on the pyrochlore lattice with first and second-neighbor exchange interactions. Ferromagnetic second-neighbor exchange $J_2 < 0$ is frustrated and lifts the vast degeneracy of the nearest-neighbor model only partially, setting stage for a nontrivial phase diagram in the (J_2, T) plane. We have used a combination of Monte Carlo simulations and analytical calculations to characterize the phases of this model. The low-temperature phase, discussed previously by Tsuneishi *et al.*,¹³ is presumably the incommensurate, and likely non-collinear, ordered phase predicted earlier by Reimers *et al.*¹² A full characterization of its magnetic order remains to be done, and its fate in the presence of strong quantum fluctuations is an interesting topic for future study.

Our simulations have uncovered the existence of another, partially-ordered phase at intermediate temperatures for a weak enough $|J_2|$. In the intermediate phase, the spins are on average collinear, which is manifested by a nonzero nematic order parameter. The order is fully characterized by a combination of a global nematic director $\hat{\mathbf{n}}$ and a 3-state Potts variable (color) on every tetrahedron indicating the location of frustrated bonds (Fig. 6). The second-neighbor interaction $J_2 < 0$ acts like an antiferromagnetic Potts coupling forcing unlike colors on neighboring tetrahedra.

The color structure of this phase resembles the BSS state²² of the antiferromagnetic Potts model: one sublattice of tetrahedra is dominated by one color (say, blue) while the other exhibits a mixture of the remaining two colors (red and green). However, unlike in the BSS state, the two colors on the second sublattice are not distributed in a completely random way: they form uniform layers in the plane coordinated with the colors (in this case, xy). The colors of individual layers appear to be random, hence *partial* order.

The partial order can be described by an individual Z_2 variable σ_i for each such layer—in addition to a global direction of the spins $\hat{\mathbf{n}}$ and the color of the other sublattice. States with different sets of $\{\sigma_i\}$ are local minima of the free energy. Accessing one such minimum from another by means of a uniform rotation of spins within one layer of tetrahedra requires climbing over a free-energy barrier that grows as the number of spins in that layer and thus becomes impossible in the thermodynamic limit. A more plausible route to changing the color of a layer is by nucleating a bubble of the opposite σ_i , which will grow if the new state has a lower free energy. Since the distinct layered states are not related by symmetry, their free energies are generally different and the nucleation route may well lead to a selection of some of these states. We have not observed such an effect in our simulations.

It is worth stressing that the ideal collinear states do not minimize the exchange energy—either globally or locally. They owe their stability to thermal fluctuations, which effectively renormalize exchange couplings and turn these spin configurations into minima of the free energy. As the temperature falls, the couplings return to their bare values and the collinear states become locally unstable at a temperature $T^* = \mathcal{O}(J_2^2/J_1)$, in agreement with our Monte Carlo simulations. The most unstable spin-wave mode has approximately the same wavenumber as the low-temperature incommensurate magnetic order. The simulated phase transition is strongly discontinuous.

Simulations on the high-temperature side show that the intermediate phase persists up to a temperature $\mathcal{O}(J_2)$. A discontinuous phase transition takes it into the paramagnetic phase. The presence of strong local spin correlations in the paramagnetic phase means that the effect of third-neighbor couplings J_3 (but not of J'_3 , see Fig. 1) is equivalent, up to a change of sign, to that of the second-neighbor coupling, at least to the first or-

der. Therefore we expect that the state of our system depends on these couplings mostly through their difference $J_2 - J_3$. If correct, this observation would extend the results of our study to a broader class of pyrochlore antiferromagnet with both J_2 and J_3 present.

Acknowledgments

It is a pleasure to thank J. Chalker and G. Jackeli for useful discussions. This work was supported in part by the NSF under Grant No. DMR-0348679 and by Research Corporation.

APPENDIX A: EQUIVALENCE OF J_2 AND $-J_3$ IN THE STRONGLY CORRELATED PARAMAGNET

At temperatures $T \ll J_1 S^2$ spins on every tetrahedron approximately satisfy the constraint

$$\sum_{i=0}^3 \mathbf{S}_i = 0. \quad (\text{A1})$$

Consider the effective magnetic field on the site labeled 3' in Fig. 1:

$$\mathbf{H}_{3'} = -\partial H / \partial \mathbf{S}_{3'} = -J_1 \mathbf{S}_0 - J_2 (\mathbf{S}_1 + \mathbf{S}_2) + \dots \quad (\text{A2})$$

where we have explicitly written out the contributions from the spins of the adjacent tetrahedron 0123. Let us now turn off the second-neighbor exchange, $J_2 = 0$, and turn on the third-neighbor coupling J_3 (Fig. 1). Doing so changes the effective field to

$$-J_1 \mathbf{S}_0 - J_3 \mathbf{S}_3 \approx -(J_1 - J_3) \mathbf{S}_0 + J_3 (\mathbf{S}_1 + \mathbf{S}_2), \quad (\text{A3})$$

where we used the constraint (A1). In this setting, a comparison of Eqs. (A2) and (A3) shows that adding a third-neighbor coupling J_3 is indeed energetically equivalent to the second-neighbor exchange of the same magnitude and opposite sign. This result does not extend to the excited states, which violate (A1), so that the physics of fluctuations need not be simply related.

APPENDIX B: CONSTRAINT ON COLORS (BOND VARIABLES)

Consider the hexagonal loop $abcdef$ shown in Fig. 14. Suppose that tetrahedra of sublattice A are in the blue state and that one tetrahedron B_1 of the other sublattice is red. Then it can be seen that tetrahedron B_2 , which has the same z coordinate, must also be red. This can be proved as follows. In the collinear state, spins can be represented by a Ising variable, i.e. $\mathbf{S}_i = \eta_i \hat{\mathbf{n}}$ and $\hat{\mathbf{n}}$ is an

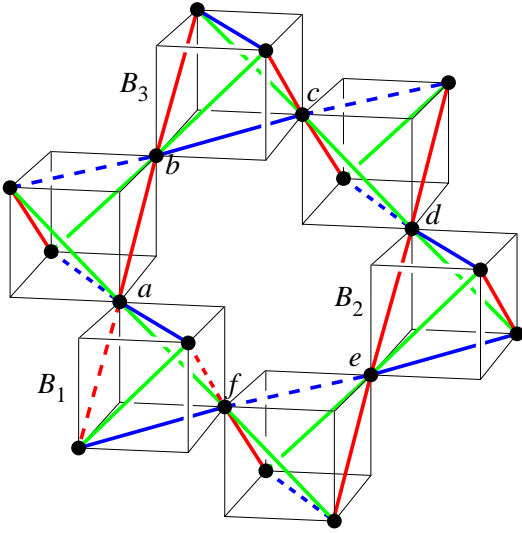


FIG. 14: A fragment of a collinear state. Frustrated bonds are shown as colored dashed lines.

arbitrary unit vector. Obviously, the product of the six bond variables $\eta_i \eta_j$ on the hexagon loop is $+1$, i.e.

$$(\eta_a \eta_b)(\eta_b \eta_c) \cdots (\eta_e \eta_f)(\eta_f \eta_a) = +1. \quad (\text{B1})$$

Among the six bonds, sublattice A contributes two antiferromagnetic and one ferromagnetic bond; this makes its total contribution $+1$. Therefore the product of the three bonds on sublattice B must be $+1$ as well. We know that $\eta_f \eta_a = +1$ (B_1 is red) and $\eta_b \eta_c = -1$ (B_3 is not blue). Hence $\eta_d \eta_e = -1$, which means that B_2 is not green. Since B_2 is not blue, it must be red.

Thus, if sublattice A is blue, the above proof shows that sublattice B has uniform color green or red in each layer $z = \text{const}$. However, the color of individual B layers are random. This is similar to the BSS phase of antiferromagnetic Potts model where individual sites on one sublattice have random colors.

APPENDIX C: MAGNETIC STRUCTURE OF THE LAYERED STATE

At the mean-field level, the collinear BSS-like states of the intermediate phase are degenerate with a larger class of layered state with non-collinear spins in general. Here we describe the magnetic structure of the general layered state.

At temperatures well below the Curie-Weiss constant, the magnetic state of a tetrahedron is determined by three staggered magnetizations \mathbf{L}_i , where $\mathbf{L}_1 = (\mathbf{S}_0 + \mathbf{S}_1 - \mathbf{S}_2 - \mathbf{S}_3)/4$, and so on.¹⁵ Here we choose to specify the Néel vectors of layers belonging to sublattice A . Because each spin is shared by two tetrahedra from different sublattices, the magnetic state of tetrahedra of sublattice B is encoded in the staggered magnetizations of the four surrounding tetrahedra of sublattice A .

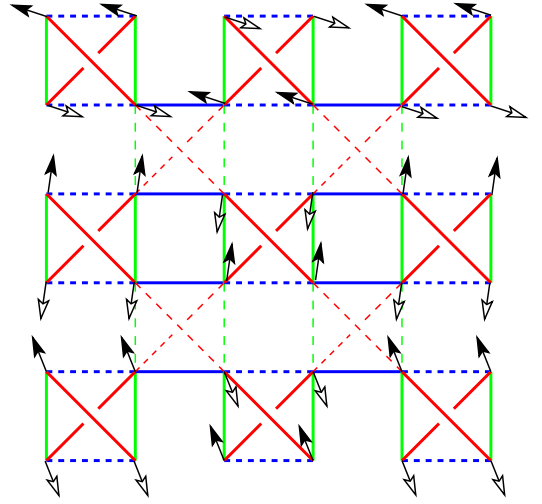


FIG. 15: Non-collinear layered state projected along the x -axis. The normal of the layers are parallel to the z axis. Frustrated bonds are shown as dashed lines.

Choosing the normal of the layers to be the z axis, the staggered magnetizations of a tetrahedron with inplane coordinate vector \mathbf{r}_\perp in the k -th layer are

$$\mathbf{L}_1 = \mathbf{L}_2 = 0, \quad \mathbf{L}_3 = \hat{\mathbf{n}}_k e^{i\mathbf{q}_\perp \cdot \mathbf{r}_\perp}, \quad (\text{C1})$$

where $\mathbf{q}_\perp = 2\pi(1,0)$ or $2\pi(0,1)$ which are equivalent with respect to the two-dimensional (2D) square lattice of tetrahedra with the same z coordinate, and $\hat{\mathbf{n}}_k$ is an arbitrary unit vector. Fig. 15 shows an example of the 2D Néel order. Once the spin order within the layers is specified, the magnetic structure of a general layered state is described by a sequence of the unit vectors $\hat{\mathbf{n}}_k$.

The bond order of the layered state is similar to the BSS state of three-state Potts model. In the example given above, sublattice A is in the collinear blue state while tetrahedra in sublattice B in general have coplanar spins; their bond order is determined by the Néel vectors of the two A layers enclosing it: $\mathbf{f}_B = \frac{4}{\sqrt{3}}(\frac{2}{\sqrt{3}}, 2\hat{\mathbf{n}}_k \cdot \hat{\mathbf{n}}_{k+1})$. For arbitrary $\hat{\mathbf{n}}_k$, the bond vector \mathbf{f}_B spreads uniformly on the edge of the triangle domain which connects the two vertices corresponding to the red and green states; the average color is again yellow.

The energy of a layered state is independent of the direction $\hat{\mathbf{n}}_k$ of spins in the individual layers:

$$E_L = -N(J_1 - 2J_2). \quad (\text{C2})$$

This energy corresponds to the extrapolated zero-temperature energy density $\varepsilon_L = -|J_2|/3$ of the nematic phase in Fig. 5. Although all layered states are degenerate at the mean-field level, thermal fluctuations apparently prefer the collinear ones as shown by the Monte Carlo simulations.

In the collinear layered states, a common direction $\hat{\mathbf{n}}$ is selected and the unit vectors $\hat{\mathbf{n}}_k \rightarrow \sigma_k \hat{\mathbf{n}}$ with the Ising variable $\sigma_k = \pm 1$. The magnetic structure of a layered

No.	Ising sequence	9	− − + + − + + +
1	+ + + + + + + +	10	− + − + − + + +
2	− + + + + + + +	11	− + + − + + − +
3	− − + + + + + +	12	− − − − + + + +
4	− + − + + + + +	13	− − − + − + + +
5	− + + − + + + +	14	− − − + + − + +
6	− + + + − + + +	15	− − + − + − + +
7	− − − + + + + +	16	− − + − + + − +
8	− − + − + + + +	17	− + − + − + − +

TABLE I: Ising sequences of the 17 distinct layered states for a pyrochlore lattice with 8 layers subject to periodic boundary conditions.

state is then specified by a sequence of Ising variables: $\{\sigma_1, \sigma_2, \dots, \sigma_k, \dots\}$. For a pyrochlore lattice with 8 layers of tetrahedra in each direction, there are 17 distinct layered states that are not related to each other by translations and inversions of the Ising variables (Table I). However, some of these states may be related by other symmetries of the lattice. For example, both states 1 and 17 represent the red-and-green state.

APPENDIX D: FREE ENERGY OF THE UNSTABLE MODE

Below we derive a Holstein-Primakoff Hamiltonian for spin waves in a state with nearly collinear spins and compute the free energy to test the local stability of the collinear state. We focus specifically on the previously identified unstable modes.

In a general state with noncollinear spins $\mathbf{S}_i = \hat{\mathbf{n}}_i$, we introduce a local reference frame defined by three orthonormal vectors: $\hat{\mathbf{e}}_i^x$, $\hat{\mathbf{e}}_i^y$, and $\hat{\mathbf{n}}_i$. A small deviation from this state could then be expressed using the Holstein-Primakoff expansion:

$$\mathbf{S}_i = \left(1 - \frac{\sigma_i^2}{2}\right) \hat{\mathbf{n}}_i + \sum_{\alpha=x,y} \sigma_i^\alpha \hat{\mathbf{e}}_i^\alpha + \mathcal{O}(\sigma^3), \quad (\text{D1})$$

Here $\sigma_i = (\sigma_i^x, \sigma_i^y)$ whose components denote fluctuation along the two orthogonal local axes. The exchange Hamiltonian then becomes

$$\mathcal{H} = \sum_{i,j} J_{ij} \hat{\mathbf{n}}_i \cdot \hat{\mathbf{n}}_j + \sum_{i,j} \sum_{\alpha,\beta} H_{ij}^{\alpha\beta} \sigma_i^\alpha \sigma_j^\beta. \quad (\text{D2})$$

with

$$H_{ij}^{\alpha\beta} = \begin{cases} -\frac{1}{2} \sum_k J_{ik} \hat{\mathbf{n}}_i \cdot \hat{\mathbf{n}}_k \delta^{\alpha\beta} & (i = j), \\ \frac{1}{2} J_{ij} \hat{\mathbf{e}}_i^\alpha \cdot \hat{\mathbf{e}}_j^\beta & (i \neq j). \end{cases} \quad (\text{D3})$$

For collinear states in the nematic phase, $\hat{\mathbf{n}}_i = \eta_i \hat{\mathbf{z}}$, and $\hat{\mathbf{e}}_i^x = \hat{\mathbf{x}}$, $\hat{\mathbf{e}}_i^y = \hat{\mathbf{y}}$, Eq. (D3) reproduces the harmonic Hamiltonian (6).

Next we compute the increase in the free energy resulting from a small deviation from a collinear state in the direction of an unstable mode of the bare Hamiltonian

(6). Let ϕ be the amplitude of the unstable mode and $\{\mathbf{m}_i\}$ the corresponding (normalized) real-space eigenvector. The deformed spin configuration is

$$\mathbf{S}_i = \hat{\mathbf{z}} \eta_i (1 - \phi^2 \mathbf{m}_i^2 / 2) + \phi \mathbf{m}_i = \hat{\mathbf{n}}_i. \quad (\text{D4})$$

Given this local spin axis, there is arbitrariness in the choice of the other two unit vectors $\hat{\mathbf{e}}_i^\alpha$. In order to apply the perturbation method, we choose:

$$\begin{aligned} \hat{\mathbf{e}}_i^x &= \hat{\mathbf{x}} \left[1 - \phi^2 \frac{(m_i^x)^2}{2} \right] - \hat{\mathbf{y}} \phi^2 \frac{m_i^x m_i^y}{2} - \hat{\mathbf{z}} \eta_i \phi m_i^x, \\ \hat{\mathbf{e}}_i^y &= -\hat{\mathbf{x}} \phi^2 \frac{m_i^x m_i^y}{2} + \hat{\mathbf{y}} \left[1 - \phi^2 \frac{(m_i^y)^2}{2} \right] - \hat{\mathbf{z}} \eta_i \phi m_i^y. \end{aligned} \quad (\text{D5})$$

Substituting these expressions into Eq. (D3), we obtain $H_{ij}^{\alpha\beta} = \delta^{\alpha\beta} H_{ij}^{(2)} + \phi^2 \Delta_{ij}^{\alpha\beta}$, where $H_{ij}^{(2)}$ is the magnon Hamiltonian of the collinear state and the perturbation $\Delta_{ij}^{\alpha\beta}$ is given by

$$\Delta_{ij}^{\alpha\beta} = \begin{cases} -\frac{1}{2} \sum_k J_{ik} [\mathbf{m}_i \cdot \mathbf{m}_k - \frac{1}{2} \eta_i \eta_k (\mathbf{m}_i^2 + \mathbf{m}_k^2)] \delta^{\alpha\beta}, & (i = j) \\ \frac{1}{2} J_{ij} [\eta_i \eta_j m_i^\alpha m_j^\beta - \frac{1}{2} (m_i^\alpha m_i^\beta + m_j^\alpha m_j^\beta)], & (i \neq j) \end{cases} \quad (\text{D6})$$

Since the bare harmonic Hamiltonian contains unstable modes as discussed in Section IV, we should replace $H_{ij}^{(2)}$ by the one renormalized by spin-wave interactions, as given in Eq. (9). We may then approximate the free energy of the system as

$$\begin{aligned} e^{-\beta F} &\approx e^{-\beta (E_L + \Lambda^* \phi^2)} \\ &\times \int' D\sigma e^{-\beta \sum_{i,j} [\tilde{H}_{ij}^{(2)} \sigma_i \cdot \sigma_j + \phi^2 \Delta_{ij}^{\alpha\beta} \sigma_i^\alpha \sigma_j^\beta]} \\ &= \tilde{Z} e^{-\beta (E_L + \Lambda^* \phi^2)} \left\langle e^{-\beta \phi^2 \sum_{i,j} \Delta_{ij}^{\alpha\beta} \sigma_i^\alpha \sigma_j^\beta} \right\rangle \\ &\approx \tilde{Z} e^{-\beta (E_L + \Lambda^* \phi^2)} e^{-\beta \phi^2 \sum_{i,j} \Delta_{ij}^{\alpha\beta} \langle \sigma_i^\alpha \sigma_j^\beta \rangle}. \end{aligned} \quad (\text{D7})$$

Here E_L is energy of the layered state, \tilde{Z} is the partition function of the renormalized Hamiltonian $\tilde{\mathcal{H}}^{(2)}$, $\langle \dots \rangle$ means Boltzmann averaging with respect to the Hamiltonian $\tilde{\mathcal{H}}^{(2)}$, and $\Lambda^* < 0$ is the bare energy of the unstable mode \mathbf{m}_i . The prime in the integral indicates that we only integrate out the low-energy magnons close to the Goldstone mode of the collinear state.

Upon expanding the fluctuations in terms of spin-wave eigenvectors $\sigma_i^\alpha = \sum_n \xi_n^\alpha u_{n,i}$, we obtain the spin correlation:

$$\begin{aligned} \langle \sigma_i^\alpha \sigma_j^\beta \rangle &= \delta^{\alpha\beta} \sum_n' \langle |\xi_n|^2 \rangle u_{n,i}^* u_{n,j} \\ &= \delta^{\alpha\beta} \sum_n' \frac{T}{\Lambda_n} u_{n,i}^* u_{n,j} = \delta^{\alpha\beta} G_{ij}. \end{aligned} \quad (\text{D8})$$

Here Λ_n is the energy of the n -th eigenmode of the renormalized Hamiltonian $\tilde{H}_{ij}^{(2)}$. Substituting this result back into Eq. (D7) yields the free energy (22) associated with the unstable mode ϕ ,

$$F \approx \text{const} + \left(\Lambda^* + \sum_{i,j} G_{ij} \Delta_{ji} \right) \phi^2 + \mathcal{O}(\phi^4), \quad (\text{D9})$$

where $\Delta_{ij} = \sum_\alpha \Delta_{ij}^{\alpha\alpha}$.

-
- ¹ R. Moessner and A. P. Ramirez, *Physics Today* **59** (2), 24 (2006).
 - ² G. H. Wannier, *Phys. Rev.* **79**, 357 (1950).
 - ³ *Physica* **16**, 425 (1950).
 - ⁴ S. T. Bramwell and M. J. P. Gingras, *Science* **294**, 1495 (2001).
 - ⁵ R. Moessner and J. T. Chalker, *Phys. Rev. B* **58**, 12049 (1998).
 - ⁶ S. V. Isakov, K. Gregor, R. Moessner, and S. L. Sondhi *Phys. Rev. Lett.* **93**, 167204 (2004).
 - ⁷ C. L. Henley, *Phys. Rev. B* **71**, 014424 (2005).
 - ⁸ C. Kittel, *Phys. Rev.* **120**, 335 (1960).
 - ⁹ O. Tchernyshyov, R. Moessner, and S. L. Sondhi, *Phys. Rev. B* **66**, 064403 (2002).
 - ¹⁰ S.-H. Lee, C. Broholm, T. H. Kim, W. Ratcliff II, and S.-W. Cheong, *Phys. Rev. Lett.* **84**, 3718 (2000).
 - ¹¹ J.-H. Chung, M. Matsuda, S.-H. Lee, K. Kakurai, H. Ueda, T. J. Sato, H. Takagi, K.-P. Hong, and S. Park, *Phys. Rev. Lett.* **95**, 247204 (2005).
 - ¹² J. N. Reimers, A. J. Berlinsky, and A.-C. Shi, *Phys. Rev. B* **43**, 865 (1991).
 - ¹³ D. Tsuneishi, M. Ioki, and H. Kawamura, *J. Phys. Condens. Matter*, **19**, 145273 (2007).
 - ¹⁴ O. Tchernyshyov, O. A. Starykh, R. Moessner, and A. G. Abanov, *Phys. Rev. B* **68**, 144422 (2003).
 - ¹⁵ G.-W. Chern, C. Fennie, and O. Tchernyshyov, *Phys. Rev. B* **74**, 060405(R) (2006).
 - ¹⁶ A. N. Yaresko, *Phys. Rev. B* **77**, 115106 (2008).
 - ¹⁷ C. L. Henley, *Phys. Rev. Lett.* **62**, 2056 (1989).
 - ¹⁸ P. M. Chaikin and T. C. Lubensky, *Principles of condensed matter physics* (Cambridge University Press, Cambridge, 2000).
 - ¹⁹ K. Hukushima and K. Nemoto, *J. Phys. Soc. Jpn.* **65**, 1604 (1996).
 - ²⁰ S. Trebst, D. Huse, and M. Troyer, *Phys. Rev. E* **70**, 046701 (2004).
 - ²¹ D. L. Bergman, R. Shindou, G. A. Fiete, and L. Balents *Phys. Rev. B* **74**, 134409 (2006).
 - ²² G. S. Grest and J. R. Banavar, *Phys. Rev. Lett.* **46**, 1458 (1981).
 - ²³ S. Lapinskas and A. Rosengren, *Phys. Rev. Lett.* **81**, 1302 (1998).
 - ²⁴ U. Hizi and C. L. Henley, *J. Phys. Cond. Matt.* **19**, 145268 (2007).